ISSN (Print) 1226-1750
ISSN (Online) 2233-6656
Journal of Magnetics 24(1), 162-167 (2019) https://doi.org/10.4283/JMAG.2019.24.1.162

Fabrication of Magnetite Nanoparticle-embedded Polystyrene Composites and Their Additive Role on the Dynamic Properties of Carbonyl Iron-based Magneto-rheological Fluids

Chun Yan Gao[1], Qi Lu[1], Hyoung Jin Choi[1]*, Nam Hui Kim[2], and Chun Yeol You[2]

[1]*Department of Polymer Science and Engineering, Inha University, Incheon 22212, Korea*
[2]*Department of Emerging Materials Science, Daegu Gyeongbuk Institute of Science & Technology, Daegu 42988, Korea*

(Received 14 July 2018, Received in final form 31 December 2018, Accepted 17 January 2019)

Magnetic Fe_3O_4@polystyrene (PS) nanoscale composite particles were fabricated using a unique Shirasu porous-glass membrane technique and used as additives to a magnetorheological (MR) suspension with magnetic carbonyl-iron (CI) particles. The morphology of the fabricated Fe_3O_4@PS composites was characterized by transmission electron microscopy. The effects of the Fe_3O_4@PS composite particle additive on its MR behavior was examined using a rotation rheometer under an applied magnetic field. The results revealed improved MR behavior, such as higher storage and loss moduli, and elastic yield stress compared to those of the pure CI-based MR suspension under an external magnetic field.

Keywords : carbonyl iron, Fe_3O_4 composite, magnetorheological, additive

1. Introduction

An actively tunable magnetorheological (MR) fluid consisting of soft-magnetic particles suspended in a non-magnetic liquid, such as mineral oil or silicone oil [1-6], has attracted considerable interest for many potential applications in mechanical engineering, biomedicine, pigments, and even in aerospace devices owing to their actively controllable capability. Upon exposure to an external magnetic field, MR fluids exhibit rapid (within milliseconds) tunable rheological properties from Newtonian fluid-like to Bingham fluid-like with a solid property.

Among the potential magnetic particles, soft magnetic carbonyl-iron (CI) microspheres, possessing a large saturation magnetization value, appropriate size, and large permeability, have attracted enormous attention. On the other hand, the use of CI particles is limited by their much higher particle density than nonmagnetic fluids, which can result in rapid sedimentation in MR fluids. To improve this sedimentation problem, several experimental methods, such as the application of a coating process onto the CI particles and the introduction of additive particles, have been attempted [7, 8]. On the other hand the coating technique is generally complex and various materials, such as carbonaceous material as fillers [9], silica particles [10], clay particles [11], thixotropic agents, and surfactants, have been used additives to solve the dispersion problem. These methods are a fast and efficiency way to enhance the repulsive interaction or decrease the distance among CI microspheres.

In this study, magnetic Fe_3O_4@PS composite particles [12], which were initially fabricated by the Shirasu porous-glass (SPG) membrane emulsification method, were applied as an additive to enhance both the dispersion state and MR efficiency of pristine CI-based MR fluids. The SPG membrane emulsification method with subsequent polymerization, which is a type of suspension polymerization, has become a research hotspot because monodisperse polymeric particles with sizes of 1-60 μm can be prepared simply by one-step polymerization using this SPG membrane technique. By adopting this SPG membrane method, styrene was removed from the microchannels of the membranes into a continuous phase by the pressure of N_2 gas initially. By rotating the continuous phase, styrene droplets of a fixed size were peeled off from the surfaces of the SPG membrane and formed a continuous phase in

*Corresponding author: Tel: +82-32-860-7486
Fax: +82-32-865-5178, e-mail: hjchoi@inha.ac.kr

This paper was presented at the IcAUMS2018, Jeju, Korea, June 3-7, 2018.

a macroemulsion. The styrene macroemulsion was then mixed with Fe_3O_4 suspension together to synthesize the Fe_3O_4@PS composite. While the Fe_3O_4@PS composite particles themselves exhibit representative MR fluid behavior with excellent dispersion stability [12], this paper introduced these particles as an additive for a widely-recognized MR suspension with CI particles using a rotation rheometer from oscillatory tests. Among their rheological characteristics, the magnetic field-dependent elastic yield stress displayed a slope of 2.0 to 1.5, showing that this MR system follows a magnetic polarization mechanism.

2. Experimental

2.1. Materials

The following chemicals were used to prepare the oleic acid coated Fe_3O_4 (OA-Fe_3O_4): ferrous chloride from Yukari, Japan; and ferric chloride, ammonium hydroxide (28 %), oleic acid (98 %), octane (99 %), and hexadecane (99 %) from Sigma-Aldrich (USA). Styrene (99 %, Sigma-Aldrich, USA), as the monomer, along with initiator and dispersant, were also used in this study. Sodium dodecyl sulfate (SDS) was used as a dispersant in the dispersion phase and potassium peroxodisulfate (KPS) was used as an initiator. CI (density of 7.81 g/cm^3, BASF, Standard CM grade, Germany) and silicone oil (kinematic viscosity of 1000 cS, 0.96 g/cm^3, Shinetsu, Japan) were then used to produce the MR fluid.

The magnetic Fe_3O_4@PS composite particles were synthesized using the methodology reported elsewhere [12, 13]. The Fe_3O_4 particles were first treated with oleic acid to synthesize the hydrophobic Fe_3O_4 nanoparticles and these particles were then admixed with a SDS solution using an ultrasonicator to complete the follow-up response. Styrene as the monomer was mixed with hexadecane and squeezed out from the SPG membrane using a N_2 gas-pressure. The two suspensions were then placed in a three-neck flask for mixing. Once the reactor was heated to 80 °C, the KPS was added as an initiator. The reactor was heated to 80 °C with stirring for 24 h. Finally, the obtained Fe_3O_4@PS particle composites were dried in a vacuum oven at 65 °C for 24 h.

2.2. Preparation of MR fluid

A CI-based MR suspension was fabricated by suspending 50 wt.% of CI particles in a medium oil, while the second MR fluid was obtained by inserting Fe_3O_4@PS nanoparticles (0.1 wt.%) as an additive. For the additive system, a weight concentration of the CI microspheres was kept the same as the first sample.

2.3. Characterization

The morphology and size distribution of the Fe_3O_4/PS composite particles were examined by transmission electron microscopy (TEM, CM-220, Phillips, Netherland). The crystallinity and chemical structure were analyzed by X-ray diffraction (XRD, DMAX-2500, Rigaku, Japan) and Fourier transform-infrared spectroscopy (FT-IR), respectively. The MR behaviors of both MR samples were tested using a parallel-plate rotation rheometer (MCR 300, Anton Parr, Austria) for various magnetic field intensities at room temperature.

3. Results and Discussion

Figure 1 presents TEM images of both Fe_3O_4 and Fe_3O_4/PS magnetic composite particles with the same resolution. The Fe_3O_4/PS magnetic composites were synthesized using the SPG membrane method via an emulsion polymerization process, in which the magnetic Fe_3O_4 particles were embedded almost completely in the PS polymeric matrix particles. The mean diameter of the Fe_3O_4/PS magnetic composites dispersed in ethyl alcohol, which was performed previously using dynamic light scattering [12], was approximately 127 nm with 85 % of the particles within the 80 to 240 nm size range.

Figure 2 presents XRD patterns of the magnetic Fe_3O_4/PS composites. The peak at $\approx 19.4°$ 2θ confirmed the amorphous state of PS, as reported previously [12]. The crystalline Fe_3O_4 particles showed peaks at 19.4, 30.1, 33.5, 43.2, 53.5, 57.1, 62.6, and 71.0° 2θ, corresponding to the (220), (311), (400), (422), (422), (511), (440), and (533) planes, respectively.

Figure 3 shows the formation of magnetic Fe_3O_4/PS composites detected by FT-IR spectroscopy. The peak at 3000 cm^{-1} was assigned to a C-H stretching vibration, and those at 2923 and 2843 cm^{-1} were attributed to the symmetric and asymmetric methylene stretching group of

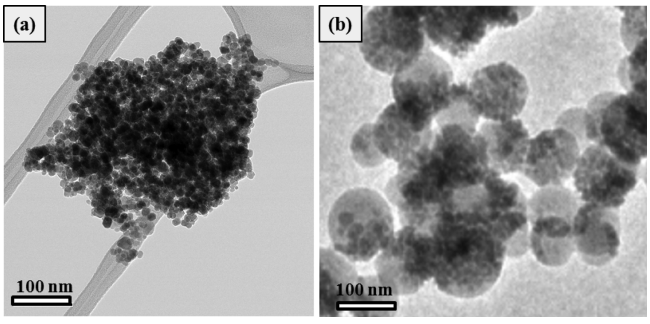

Fig. 1. TEM images of (a) Fe_3O_4 and (b) Fe_3O_4/PS magnetic composites.

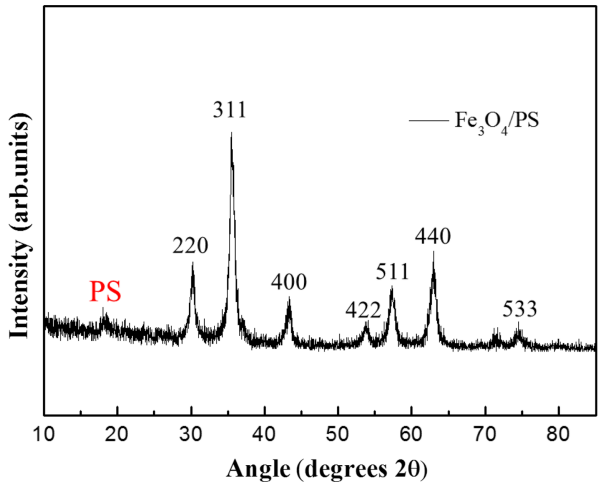

Fig. 2. (Color online) X-ray powder diffraction (XRD) profiles of Fe_3O_4/PS magnetic composites.

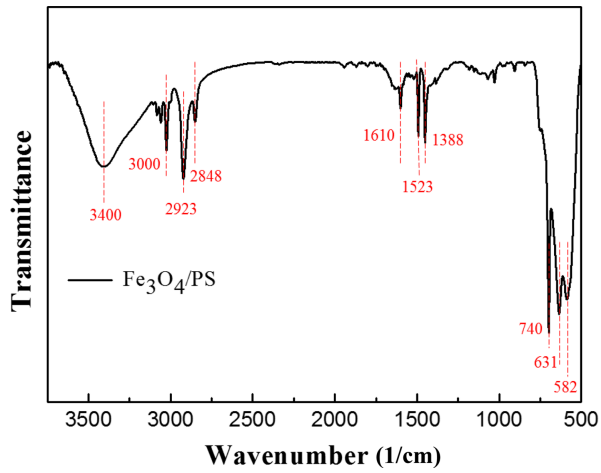

Fig. 3. (Color online) Fourier transform-infrared spectroscopy (FT-IR) of Fe_3O_4/PS magnetic composites.

PS, as reported previously [12], or to oleic acid that had been applied to modified Fe_3O_4 [14, 15]. The C=C stretching (1610 cm^{-1}) and C=O stretching bands of the carboxylate group due to symmetric (1388 cm^{-1}) and asymmetric (1523 cm^{-1}) vibration were verified. In addition, the C-H out-of-plane bending vibration of the phenyl group was observed at 740 cm^{-1} and the bands at 582 and 631 cm^{-1} were assigned to the Fe-O stretching bands in Fe_3O_4 nanoparticles [16].

The viscoelastic properties under different magnetic field strengths were tested using the dynamic oscillation method at strains ranging from 0.001 to 100 % at a constant frequency (ω = 6.28 rad/s). During the oscillation measurement process, the magnetic particles formed fibrous (or chain)-like structures vertical to the flow direction generated by a parallel-plate typed rheometer that were

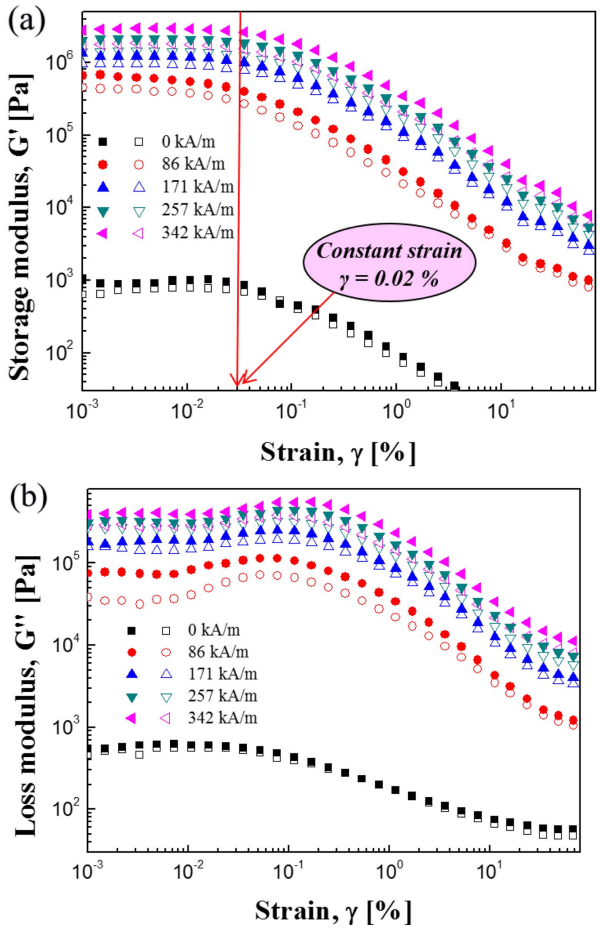

Fig. 4. (Color online) Storage (a) and loss (b) modulus for CI/Fe_3O_4@PS (filled symbol) and CI (open symbol) based MR fluid.

attributed to polarized interactions among the particles under an external magnetic field. Figure 4 presents the storage (G') and loss moduli (G'') of the CI particle-based MR suspensions with or without the Fe_3O_4@PS composite additive versus the shear strain curves. The G' and G'' values of the CI/Fe_3O_4@PS-based MR suspension were larger than those of the pristine CI-based MR fluid regardless of whether or not a magnetic field had been applied. Under an applied magnetic field, both G' and G'' increased dramatically and then increased stepwise with increasing magnetic field strength. When the shear strain was smaller than the critical value, both the storage and loss moduli exhibited an almost plateau region known as the linear viscoelastic region (γ_{LVE}), where fibrous-like structures were quite stable. Thus, a constant strain of 0.02 % was chosen for further frequency sweep measurements. As soon as the strain reached a critical value, G' and G'' decreased suddenly as the strain was increased due to irreversible deformation of the MR fluid from the chain-like structure to the liquid-like structure-based MR fluid

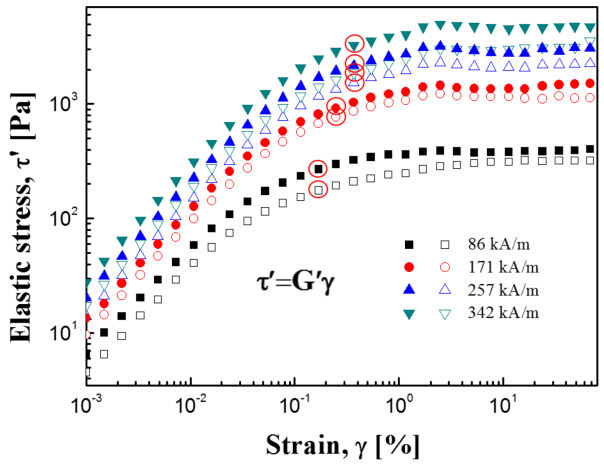

Fig. 5. (Color online) Elastic stress for CI/Fe_3O_4@PS (filled symbol) and CI (open symbol) based MR fluids as a function of strain.

even in the absence of an external magnetic field [17, 18].

The strain-dependent elastic stress, $\tau' = G'\gamma$, under a series of applied extra magnetic field strengths in log-log coordinates were determined using the data from Fig. 4, as shown in Fig. 5. In the minor strain region, the elastic yield stress increased almost linearly with increasing strain, where the MR suspensions could recover to their original phase after removing the stress. When the applied stress exceeded an elastic yield stress value, MR fluids showed an irreversible change, in which the rate of stress growth decreased gradually, emerging as a plateau plastic range.

Figure 6 shows magnetic field-dependent elastic yield stresses (τ_y) for both CI/Fe_3O_4@PS and CI-based MR fluids on a logarithmic scale, which were obtained from

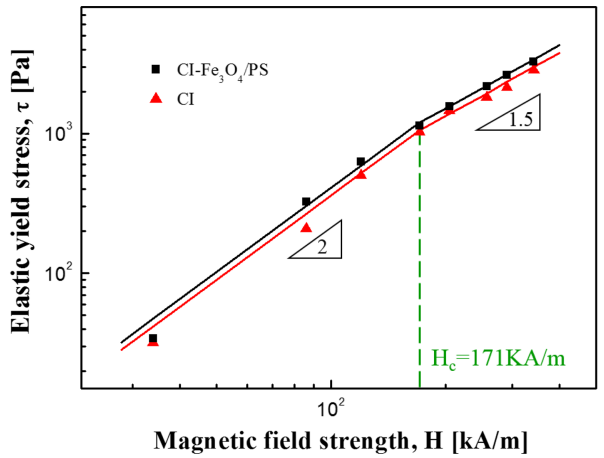

Fig. 6. (Color online) Elastic yield stress for CI/Fe_3O_4@PS (black square) and CI (red triangle)-based MR fluids as a function of magnetic field strengths.

the first deflection point of the elastic stress in Fig. 5 under different magnetic field strengths. Compared to their dynamic yield stresses obtained from a steady shear test [13], the elastic yield stresses were lower. When the H value is smaller than the critical magnetic field strength, H_c, τ_y is proportional to H^2 [19, 20], as shown in Eq. (1):

$$\tau_y \propto H^2 \tag{1}$$

The polarization force increases with increasing H, which is beneficial to forming a chain-like structure in a MR fluid. On the other hand, when $H > H_c$, the MR fluid reaches the local saturation of magnetization and the relationship between τ_y and H can be described in Eq. (2):

$$\tau_y \propto H^{1.5} \tag{2}$$

In addition, a universal yield stress formula has been recommended to assess a MR suspension in the presence of extra magnetic field strengths, as shown in Eq. (3) [21], which is analogous to the electrorheological suspensions in external electric fields [22]:

$$\tau_y(H) = \alpha H^2\left(\frac{\tanh\sqrt{H/H_c}}{\sqrt{H/H_c}}\right) \tag{3}$$

The parameter, α, is related to the volume concentration of the MR system and susceptibility. Based on Eq. (3), the yield stress (τ_y) could present two limiting conditions with respect to H, as shown as Eq. (4):

$$\begin{aligned} \tau_y &= \alpha H^2 \qquad H << H_c \\ \tau_y &= \alpha\sqrt{H_c}H^{3/2} \qquad H >> H_c \end{aligned} \tag{4}$$

Through further analysis, a generalized formula could be estimated by H_c and its corresponding yield stress of $\tau_y(H_c) = 0.762\,\alpha H_c^2$. When $\hat{H} \equiv \frac{H}{H_c}$ and $\hat{\tau} \equiv \frac{\tau(H)}{\tau(H_c)}$ were applied to Eq. (3), a new universal equation was obtained as follows:

$$\hat{\tau} = 1.313\hat{H}^{3/2}\tanh\sqrt{\hat{H}} \tag{5}$$

Therefore, the elastic yield stress curves can merge into a single line via Eq. (5), as shown in Fig. 7, which is similar to that obtained from their dynamic yield stress [13].

To further demonstrate the characteristics of MR suspensions, an angular frequency sweep test of the CI/Fe_3O_4@PS (filled) and CI (open)-based MR suspensions with a constant amplitude of 0.02 % and a frequency ranging from 1 to 100 rad/s was performed in the presence or absence of a magnetic field, as shown in Fig. 8. At zero magnetic field, both the CI/Fe_3O_4@PS and neat CI-based MR suspension exhibited typical Newton fluid-

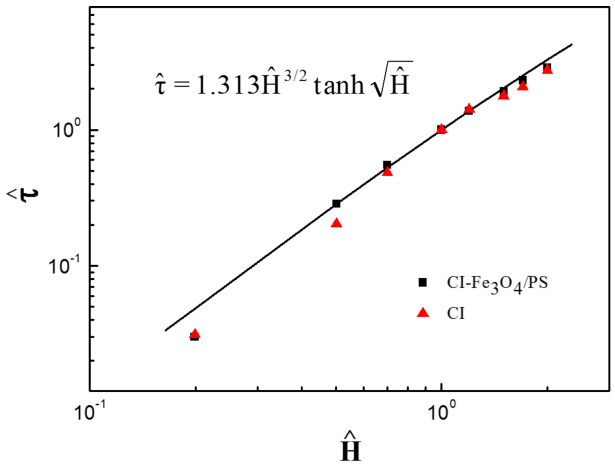

Fig. 7. (Color online) $\hat{\tau}$ for CI/Fe_3O_4@PS (black square) CI (red triangle) based MR fluids as function of $\hat{H}$. Solid line in plot is fitting by Eq. (5).

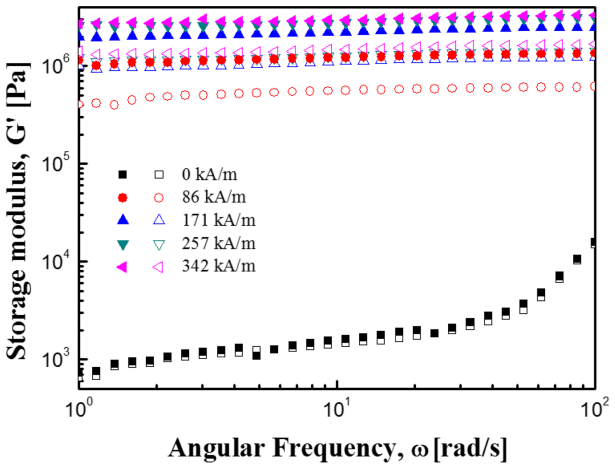

Fig. 8. (Color online) Frequency sweep of storage moduli for CI/Fe_3O_4@PS (filled symbol) and CI (open symbol)-based MR fluids with a constant amplitude of 0.02 %.

like behavior in that the G' value increases with increasing angular frequency. After applying the magnetic field, the storage modulus improved almost instantaneously by three orders of magnitude followed by a stepwise increase. The G' values of the MR fluid with the additive were always were higher than that of neat CI under the same magnetic field and angular frequency [23].

The stress relaxation property of the MR fluids also plays a major role in describing the behavior of MR fluids, as indicated in Fig. 9, where the significant state change from fluid-like to solid-like was observed after applying the magnetic fields. The shear relaxation modulus $G(t)$ of both CI/Fe_3O_4@PS (filled) and CI (open)-based MR suspensions as a function of time could be deduced from both G' and G'' with a functional relation in Eq. (6) known

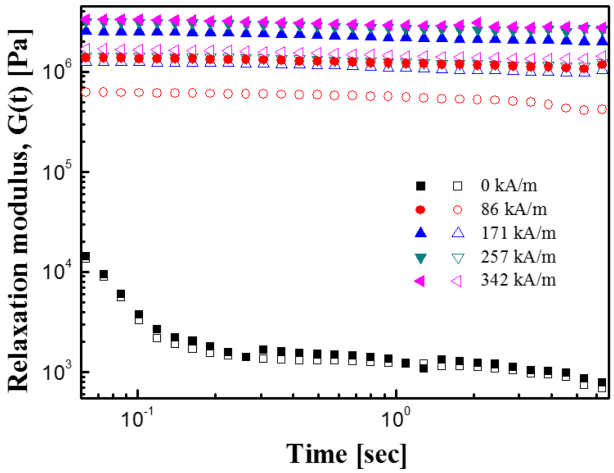

Fig. 9. (Color online) Relaxation modulus of the CI/Fe_3O_4@PS (filled symbol) and CI (open symbol)-based MR fluids.

as the Schwarzl equation [24]:

$$G(t) \cong G'(\omega) - 0.566G''(\omega/2) + 0.203G''(\omega) \quad (6)$$

In the absence of a magnetic field, the liquid-like phase of the MR suspension was confirmed with or without the Fe_3O_4@PS composites. In the presence of a magnetic field, however, the relaxation modulus exhibited a plateau versus time in a logarithmic relationship caused by the strong and stable attraction among the magnetic beads under a fixed magnetic field strength.

Figure 10 shows the MR efficiency calculated from $(G' - G_0')/G_0$, where G' is the storage modulus of the MR fluid in the presence of an applied magnetic field strength and G_0' is the initial storage modulus under a zero magnetic field [25, 26]. With increasing magnetic field strength from 86 to 342 kA/m, the MR efficiency increased over the entire region and the values of the CI/Fe_3O_4@PS MR fluid were always higher than those of the

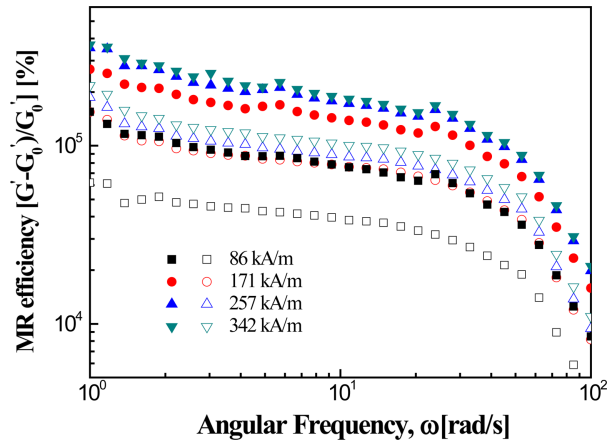

Fig. 10. (Color online) MR efficiency of the CI/Fe_3O_4@PS (filled symbol) and CI (open symbol)-based MR fluids.

CI MR suspension at the same field strength, meaning that the additive can improve the MR efficiency. Under the same magnetic field, the MR efficiency decreased with increasing angular frequency because the deformed chain structure of the magnetic particles resulted in a weak flow resistance [27].

4. Conclusion

Nanoscale Fe_3O_4@PS composite particles were fabricated using a SPG membrane method and then adopted to a CI-based MR suspension as an additive. The viscoelastic behaviors of the CI/Fe_3O_4@PS-based MR fluid were enhanced compared to the neat CI-based MR suspension under an external magnetic field from both the controlled strain sweep and controlled frequency sweep test. The elastic yield stresses and magnetic-field dependence were analyzed using a universal yield stress function, showing a change in slope from 2.0 to 1.5. Higher MR efficiency for the CI/Fe_3O_4@PS-based MR suspension was also observed over a wide frequency range.

Acknowledgement

This study was supported by the research grant from National Research Foundation of Korea (2018R1A4A 1025169).

References

[1] M. Mrlik, M. Ilcikova, V. Pavlinek, J. Mosnacek, P. Peer, and P. Filip, J. Colloid Interface Sci. **396**, 146 (2013).
[2] D. J. Klingenberg and J. C. Ulicny, Int. J. Modern Phys. B **25**, 911 (2011).
[3] M. Ashtiani and S. H. Hashemabadi, Colloids Surf. A **469**, 29 (2015).
[4] L. Tan, H. T. Pu, M. Jin, Z. H. Chang, D. C. Wan, and J. L. Yin, Colloids Surf. A **360**, 137 (2010).
[5] B. J. Park, F. F. Fang, and H. J. Choi, Soft Matter **6**, 5246 (2010).
[6] Y. M. Han, S. Kim, Y. D. Park, J. W. Kamg, and S. B. Choi, Smart Mater. Struct. **24**, 115016 (2015).
[7] W. L. Zhang, S. D. Kim, and H. J. Choi, IEEE Trans. Magn. **50**, 2500804 (2014).
[8] I. Bica, E. M. Anitas, and L. Chirigiu, J. Ind. Eng. Chem. **56**, 407 (2017).
[9] I. Bica, E. M. Anitas, L. M. E. Averis, and M. Bunoiu, J. Ind. Eng. Chem. **21**, 1323 (2015).
[10] X. Zhang, W. Li, and X. Gong, Smart Mater. Struct. **19**, 125012 (2010).
[11] M. T. Lopez-Lopez, A. Gomez-Ramirez, J. D. G. Duran, and F. Gonzalez-Caballero, Langmuir **24**, 7076 (2008).
[12] C. Y. Gao, M. W. Kim, D. H. Bae, Y. Z. Dong, S. H. Piao, and H. J. Choi, Polymer **125**, 21 (2017).
[13] C. Y. Gao, Q. Lu, and H. J. Choi, IEEE Trans. Magn. **54**, 4600904 (2018).
[14] S. H. Kwon, Y. D. Liu, and H. J. Choi, J. Colloid Interface Sci. **440**, 9 (2015).
[15] K. Yang, H. Peng, Y. Wen, and N. Li, Appl. Surf. Sci. **256**, 3093 (2010).
[16] L. Cui, H. Xu, P. He, K. Sumitomo, Y. Yamaguchi, and H. Gu, J. Polym. Sci. Part A: Polym. Chem. **45**, 5285 (2007).
[17] K. J. Son, Korea-Austral. Rheol. J. **30**, 29 (2018).
[18] Y. Seo and H. J. Choi, Korea-Austral. Rheol. J. **30**, 317 (2018).
[19] J. M. Ginder, L. C. Davis, and L. D. Elie, Int. J. Mod. Phys. B **10**, 3293 (1996).
[20] M. J. Hato, H. J. Choi, H. H. Sim, B. O. Park, and S. S. Ray, Colloids Surf. A **377**, 103 (2011).
[21] F. F. Fang, H. J. Choi, and M. S. Jhon, Colloids Surf. A **351**, 46 (2009).
[22] Y. D. Liu, B. J. Park, Y. H. Kim, and H. J. Choi, J. Mater. Chem. **21**, 17396 (2011).
[23] Y. P. Seo, S. Han, J. Choi, A. Takahara, H. J. Choi, and Y. Seo, Adv. Mater. **30**, 1704769 (2018).
[24] I. Emri, B. S. von Bernstorff, R. Cvelbar, and A. Nikonov, J. Non-Newton. Fluid Mech. **129**, 75 (2005).
[25] A. Lengalova, V. Pavlinek, P. Saha, O. Quadrat, T. Kitano, and J. Stejskal, Eur. Polym. J. **39**, 641 (2003).
[26] M. Sedlacik, V. Pavlinek, P. Saha, P. Svrcinova, P. Filip, and J. Stejskal, Smart Mater. Struct. **19**, 115008 (2010).
[27] J. Yin, Y. Shiu, Y. Dong, and X. Zhao, Nanotechnology **25**, 045702 (2014).